DOI: 10.1002/chem.200700763

Alkali Metal Diphenylmethanides: Synthetic, Computational and Structural Studies

Jacob S. Alexander, Damian G. Allis,* Weijie Teng, and Karin Ruhlandt-Senge*[a]

Abstract: In search of new synthetic precursors for the preparation of alkaline earth organometallic compounds, we investigated the application of a powerful desilylation reaction to cleanly afford a variety of contact and charge-separated alkali metal derivatives without the difficulties commonly encountered in other methods. The resulting diphenylmethanides display both contact molecules and separated ion pairs. Analysis of the structural data demonstrates that simple electrostatic models are insufficient for predicting and explaining the solid-state structures of these complexes. Detailed computational investigations were performed to probe the nature of the metal–anion and metal–donor interactions and determine the contributions of each to the observed solid-state structures.

Keywords: alkali metals · density functional calculations · diphenylmethanides · ion association · structure elucidation

Introduction

The importance of alkali organometallic compounds cannot be overstated, especially complexes with a host, which have far reaching applications. These have been summarized in several reviews.[1–5] In addition to their value in organic synthesis, the target molecules have shown enormous utility in the preparation of a range of organometallic compounds through salt metathesis reactions via the potassium salts[6] and are discussed as reactive intermediates in superbase chemistry.[7] Due to the interesting structural features displayed by many of these compounds, theoretical studies have focused on the various metal–ligand binding modes, resulting in considerable theory, focusing primarily on rationalizing metal–ligand binding trends and the degree of σ- or π-bonding in these systems.[4,8–15] Even with significant attention focused on the alkali metal derivatives, the limited range of preparative methods and difficulties regarding stability and solubility have prevented the investigation of several worthwhile ligand systems. Particularly interesting among these is the diphenylmethanide anion. Vigorous study has encompassed substituted phenylmethanes (particularly the benzyl and triphenyl systems), yet scant information exists on this logical fit into the hierarchy.

While some combinations of alkali phenylmethanes have been well-investigated, few structurally characterized examples, including several unsubstituted benzyl derivatives such as $[Li(OEt_2)_2(C_7H_7)]_n$,[16] $[Na(tmeda)(C_7H_7)]_4$,[17] and $[M(pmdta)(C_7H_7)]$,[15,18] (M = Na, K, Rb) (TMEDA = *N*,*N*,*N*′,*N*′-tetramethylethylene diamine) (PMDTA = *N*,*N*,*N*′,*N*′,*N*″-pentamethyldiethylenetriamine) are available. Triphenylmethanides have been the subject of structural and computational investigations, with structural data available for the charge-separated lithium triphenylmethanide [Li([12]crown-4)][CPh_3)],[19] the TMEDA and PMDTA adducts [M(tmeda)(CPh_3) (M = Li, Na)[20,21] and [M(pmdta)(CPh_3)] (M = K, Rb, Cs)[14] as well as several other potassium salts with varying donors.[22] In contrast, similar work on the diphenylmethanides is almost nonexistent, with only the charge-separated [Li[12]crown-4)][($HCPh_2$)],[19] the polymeric $[Na(tmeda)(HCPh_2)]_n$ and the monomeric [Na(pmdta)($HCPh_2$)] known.[18]

Major impediments to the preparation of alkali organometallics are low solubility and stability, particularly in ethereal solvents. While the preparation of the lithium congeners is generally straightforward due to the ready availability of lithiated starting materials such as *n*BuLi, synthetic strategies for heavy alkali metal complexes are more complex.

[a] Dr. J. S. Alexander, Dr. D. G. Allis, Dr. W. Teng, Prof. Dr. K. Ruhlandt-Senge
Department of Chemistry
1-014 Center for Science and Technology, Syracuse University
Syracuse, New York 13244-4100 (USA)
Fax: (+1) 315-443-4070
E-mail: damian@somewhereville.com
kruhland@syr.edu

Supporting information for this article is available on the WWW under http://www.chemeurj.org/ or from the author.

The most commonly employed method involves the combined use of an organolithium with an alkali alkoxide reagent, also often called "superbase" chemistry, see Equation (1).[7]

$$RH + MO\textit{t}Bu/\textit{n}BuLi \xrightarrow{M=Na,\ K,\ Rb,\ Cs} MR + LiO\textit{t}Bu + C_4H_{10} \quad (1)$$

While a powerful entry, this method is limited in several respects. First, due to the highly basic nature of the metallating reagent, metallation is not always selective. Second, in order for the reaction to proceed at a reasonable rate, homogeneous reaction conditions are required, demanding the use of ethereal solvents that necessitate low reaction temperatures to avoid ether cleavage. Finally, depending on the ligands employed, lithium alkoxides can be difficult to separate from the target compound, even with repeated washings and/or recrystallizations.[23] Because of these limitations, we developed a rational method to enable the clean, facile preparation of heavy alkali metal organometallics. Shown here for diphenylmethanides, this method will cleanly afford secondary alkali metal organometallics through simple desilylation chemistry.

This work closely connects to previous work in our laboratory concerned with rubidium diphenylmethanides. These compounds in the presence of [18]crown-6 display two different metal-binding modes in the solid-state (η^3 and η^6), depending on the crystallization temperature.[24] These compounds are included here (**9**, **10**) as a point of reference. An additional motivation for our work is the examination of ion association and relationship between charge density and preference for σ- or π-binding in the target compounds, both major contributors to the synthetic capabilities of organoalkali metal compounds. To this effect, we prepared diphenylmethanides of different alkali metals and introduced crown ethers of various diameters.

This work significantly increases the range of synthetic tools and the library of known alkali metal organometallics. Included in this work are the syntheses and characterization of the charge-separated compounds [K[18]crown-6)(thf)$_2$][HCPh$_2$] (**1**), [Cs$_2$[18]crown-6)$_3$][HCPh$_2$]$_2$ (**2**), [Rb[15]crown-5)$_2$][HCPh$_2$] (**3**), [K[15]crown-5)$_2$][HCPh$_2$] (**4**), [Rb[12]crown-4)$_2$][HCPh$_2$] (**5**), [K[2.2.2]cryptand][HCPh$_2$] (**6**), [Rb[2.2.2]cryptand][HCPh$_2$] (**7**) and the contact pairs [Cs[2.2.2]cryptand][HCPh$_2$] (**8**), and the previously reported η^3[Rb[18]crown-6][HCPh$_2$] (**9**) and η^6[Rb[18]crown-6-(thf)HCPh$_2$] (**10**),[24] that are included in the discussion. Our synthetic and spectroscopic studies are supplemented by theoretical work geared to reveal the energetic profiles of metal ligand binding. To this effect, quantum chemical computations more detailed than previously reported for **9** and **10** are included.

Results

Synthetic aspects: A recent report of lithium derivatives of trimethylsilyl substituted diphenylmethanide[25] led to the intriguing possibility of employing a technique noted for the preparation of alkali metal silanides and phosphides taking advantage of the relative weakness of the phosphorus-silicon or silicon-silicon bond and the stability of silyl ethers [Eq. (2a,b)]:[26–28]

$$P(SiMe_3)_3 + KO\textit{t}Bu \rightarrow KP(SiMe_3)_2 + SiMe_3\text{-}O\textit{t}Bu \quad (2a)$$

$$Si(SiMe_3)_4 + KO\textit{t}Bu \rightarrow KSi(SiMe_3)_3 + SiMe_3\text{-}O\textit{t}Bu \quad (2b)$$

Employed as an entry into alkali organometallic compounds, this method would allow for the facile preparation of the target compounds while avoiding many of the pitfalls associated with other methods. Although the lithium diphenylmethanides reported were prepared via direct metallation reactions under retention of $SiMe_3$,[25] it was expected that the greater ionic nature of the heavier alkali metal alkoxides would instead promote the $SiMe_3$ cleavage reactions observed for the phosphides and silanides. Consequently, the formation of alkali organometallics by addition of a heavy alkali metal alkoxide to a silylated diphenylmethanide, assisted by an appropriately sized crown ether, should be driven by the formation of silyl ether as well as resonance in the planarized anion to form the desired products [Eq. (3)]:

$$HCPh_2SiMe_3 + MO\textit{t}Bu \xrightarrow[M=Na,\ K,\ Rb,\ Cs]{donor} M(donor)CHPh_2 + SiMe_3\text{-}O\textit{t}Bu \quad (3)$$

The advantages of this reaction would include work at ambient reaction conditions by using hydrocarbon solvents, thus circumventing undesirable side reactions, while improving the yield and purity of the target compounds. Moreover, no difficulties separating the solid and side products are to be expected.

Treatment of diphenyltrimethylsilylmethane with an equivalent of alkali metal *tert*-butoxide in the presence of complexing crown ether cleanly affords a family of alkali metal diphenylmethanides. All compounds could be obtained in good yield and purity through reaction in hexane. The resulting products were recrystallized from hexane/THF to afford crystals suitable for X-ray diffraction studies.

Compounds **1–10** were characterized by using single crystal X-ray diffraction to identify the metal–ligand bonding characteristic data. NMR spectroscopic studies complement the solid-state work, obtaining a glimpse of the ion association in solution.

Crystallographic Studies

Compounds **1–7** display separated ions in the solid-state, whereas **8–10** crystallize as contact molecules.

In most of the compounds presented here, conformational disorder in the diphenylmethanide unit is observed (Figure 1). In this "flip" disorder, the anion adopts two separate orientations which may or may not involve a center of symmetry.

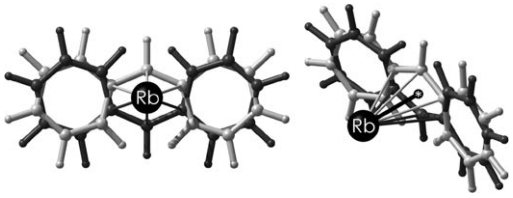

Figure 1. Representation demonstrating two orientations of anion "flip" disorder.

This disorder is manifest particularly in the charge-separated structures, although in one instance it is noted for a contact molecule (**8**) (see below). Generally, the disorder was modeled by treating each orientation of the anion (one with the methylene pointing "up" and one "down" as a whole), and allowing the two occupancies to refine freely. Typically, occupancies were centered very close to 50:50. The two orientations are not exactly identical, but closely related. Therefore, only the major (or one of the two equally occupied) orientation is listed in tables and mentioned in the discussion. Overall, the anion geometry is very similar for the separated ions **1**–**7**, so only one general description is provided for all compounds. Geometrical data for the anions reported as well as several previously prepared relevant compounds are summarized in Table 1.

The anions display resonance-stabilized, planar geometries with C_{phenyl}-C_{ipso}-C_{phenyl} angles in the range of 131 to 133°, which demonstrates the increased steric demand of a phenyl (as in CPh_3^-) as compared to a hydrogen substituent (as in $CHPh_2^-$). This widening allows for the phenyl rings to be close to coplanar in each example, although some minor ring twisting (ca. 5°) is observed in some examples. These data do not agree with an earlier MNDO theory prediction of phenyl twisting of 25°.[29]

Generally, the diphenylmethanide anion adopts a geometry that is planar through the central methylene carbon with none of the pyramidalization observed for the lighter congeners of alkali triphenylmethanides and for alkali methyl derivatives.[2,20,21] In all cases the anion demonstrates the expected resonance stabilization, although a slight elongation of the C_{ipso}–C_{ortho} bonds consistent with previous related anions[18,19] is visible. Those are most pronounced in the cesium species **2** and **8**, with values of 1.396(10) Å for **8** and expansion to as much as 1.445(4) Å for **2**; although some of this elongation may be the result of anion disorder (and consequent increase in uncertainly of atom positions), but significant bond localization, as observed in a family of alkali bisdipyridylmethanides (see below)[12,13] does not appear to be present.

Crown ether and cryptand coordination of the alkali metals are the overlying structure-determining elements in the compounds reported. Extensive structural data are available on the macrocycle coordination to alkali metals, but their detailed influence on the ion association in organometallic compounds remains to be fully understood. Well-documented cation/macrocycle matches such as potassium or barium and [18]crown-6 afford full encapsulation of the cation by the crown cavity; the apical positions were filled

Table 1. C–C distances [Å] in the diphenylmethanide anion.

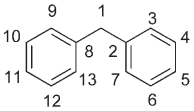

Compound	C2–3, C8–9	C3–4, C9–10	C4–5, C10–11	C5–6, C11–12	C6–7, C12–13	C7–2, C13–8
[Li([12]crown-4)$_2$][HCPh$_2$]	1.433(6), 1.423(6)	1.399(7), 1.372(6)	1.429(5), 1.365(6)	1.367(5), 1.375(6)	1.377(6), 1.360(5)	1.438(6), 1.430(7)
[Na(pmdta)][HCPh$_2$][a]	1.424(6), 1.432(7), 1.446(7), 1.389(7)	1.381(7), 1.369(8), 1.369(7), 1.361(7)	1.378(7), 1.384(7), 1.378(7), 1.346(7)	1.372(6), 1.383(7), 1.364(7), 1.402(7)	1.364(7), 1.377(7), 1.325(8), 1.370(8)	1.431(7), 1.396(6), 1.397(7), 1.439(7)
[Na(HCPh$_2$)(tmeda)]$_4$[c]	1.43(1), 1.43(1)	1.35(1), 1.39(1)	1.37(1), 1.34(2)	1.38(1), 1.40(1)	1.35(2), 1.40(2)	1.42(1), 1.40(1)
K[2.2.2]cryptand(HCPh$_2$)	1.420(5), 1.419(5)	1.292(14), 1.484(14)	1.55(2), 1.25(2)	1.376(11), 1.408 (10)	1.371(6), 1.382(5)	1.433(6), 1.419(5)
[K[18]crown-6(thf)$_2$][HCPh$_2$]	1.432(12), 1.42(2), 1.30(2), 1.41(2)	1.51(3), 1.362(16), 1.39(3), 1.339(13)	1.43(3), 1.44(2), 1.30(3), 1.28(2)	1.39(2), 1.40(2), 1.39(2), 1.28(2)	1.333(15), 1.352(15), 1.40(2), 1.38(2)	1.447(13), 1.417(14), 1.405(14), 1.44(3)
η^3-[Rb[18]crown-6][HCPh$_2$]	1.413(6), 1.431(6)	1.358(6), 1.416(5)	1.365(6), 1.378(5)	1.358(6), 1.386(5)	1.396(6), 1.378(5)	1.423(7), 1.352(5)
η^6-[Rb[18]crown-6][HCPh$_2$]	1.449(13), 1.405(14)	1.356(13), 1.371(14)	1.381(15), 1.375(17)	1.414(15), 1.387(17)	1.362(14), 1.378(16)	1.397(13), 1.427(14)
[Rb([12]crown-4)$_2$][HCPh$_2$]	1.422(4), 1.435(4)	1.379(4), 1.373(4)	1.382(4), 1.394(4)	1.390(4), 1.390(4)	1.383(4), 1.374(5)	1.422(4), 1.423(4)
[Rb[2.2.2]cryptand][HCPh$_2$][b]	1.410(8), 1.432(6)	1.39(2), 1.381(7)	1.404(17), 1.392(16)	1.387(6), 1.37(2)	1.385(6), 1.387(8)	1.425(6), 1.421(5)
[Cs$_2$([18]crown-6)$_3$]-[HCPh$_2$]$_2$[a]	1.415(4), 1.445(4), 1.430(9), 1.416(4)	1.372(5), 1.363(4), 1.389(15), 1.403(4)	1.413(5), 1.389(5), 1.402(12), 1.409(5)	1.372(4), 1.380(4), 1.379(9), 1.405(5)	1.372(4), 1.373(4), 1.375(10), 1.409(5)	1.400(4), 1.412(4), 1.415(9), 1.413(4)
[Cs[2.2.2]cryptand][HCPh$_2$][b]	1.396(10)	1.345(13)	1.380(17)	1.386(13)	1.378(10)	1.487(11)

[a] Two independent anions. [b] Half anion is symmetry equivalent. [c] Tetrameric structure; representative anion listed here.

by ligand molecules as demonstrated in [Ba[18]crown-6]-[$(CHPh_2)_2$].[30] For the alkali metals, the second apical coordination may be filled by a donor molecule. However, if the metal diameter is larger than the crown cavity, steric shielding provided by the macrocycle becomes less effective, since the metal is located above the plane of crown donor atoms. This arrangement typically results in the coordination of a second macrocycle under formation of a sandwich complex. In contrast, ligand coordination in order to sterically satisfy the metal coordination sphere is rarely effective in those cases.

Compound **1** (Figure 2) crystallizes with two independent molecules, with the cation positioned approximately in the center of the crown ether rings with THF molecules filling

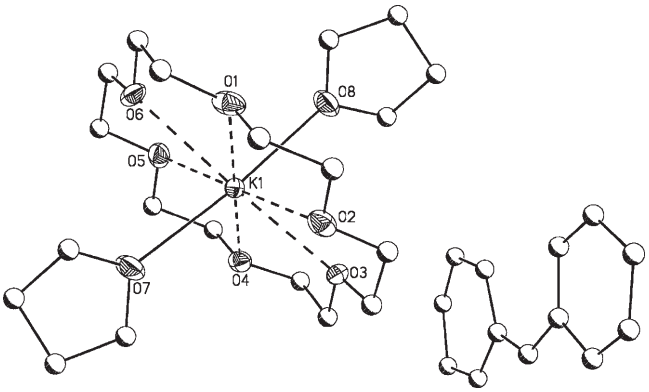

Figure 2. Crystal structure of **1**. Non-carbon atoms shown as thermal ellipsoids at 30% probability. Hydrogen atoms have been removed for clarity.

the axial vertices. This provides a favorable space filling arrangement at potassium, and thus promotes the formation of separated ions. The metal coordination number is 8, with unexceptional metal–oxygen (crown) bond lengths ranging from 2.733(5) to 2.845(5) Å; metal–THF distances are slightly shorter (2.67–2.71(4) Å). It is instructive to compare the charge-separated [K[18]crown-6$(thf)_2$][$HCPh_2$] with the previously reported [Ba[18]crown-6][$(HCPh_2)_2$].[30] Despite very similar ionic radii (1.38 (K^+) vs 1.35 Å (Ba^{2+}) for six-coordinate species)[31] the compounds do not adopt the same ion association mode, rather the slightly smaller, more polarizing barium center prefers coordination to the anionic ligands. With a reduced charge density, the slightly larger potassium cation is sufficiently stabilized by metal–donor interactions, a result confirmed by previous theoretical studies.[32]

Separated ions are also observed in the cesium diphenylmethanide **2** (Figure 3), where the two cesium atoms adopt a charge-separated "double sandwich" structure with three crown ethers, thus ensuring the steric saturation of the large cesium centers. The outer crown ether rings lie at distances ranging from 3.081(2)–3.341(2)°. As expected, the inner bridging ring lies noticeably farther from the metal centers at distances from 3.302(3)–3.760(3)°. This double sandwich structure is a desired synthetic target because of its ability to stabilize large, negatively charged complexes, with previous applications in cluster chemistry,[33,34] and to a lesser extent transition-metal chemistry.[35,36] Still, structurally characterized examples of this system with simple organic anions are rare.[37–40]

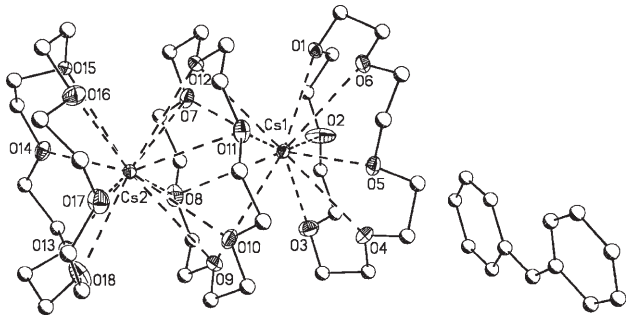

Figure 3. Crystal structure of **2**. Non-carbon atoms shown as thermal ellipsoids at 30% probability. Hydrogen atoms have been removed for clarity. Only one anion is shown.

The charge-separated rubidium and potassium species **3** (Figure 4) and **4** display very similar structural features with the metal centers fully encapsulated by two [15]crown-5 macrocycles. However, significant disorder in **4** did not allow for a satisfactory data refinement, but there is no doubt as to the overall structural features or the chemical makeup. The identity of **4** is further confirmed via ^1H and ^{13}C NMR spectroscopic data. The rubidium–oxygen distances in **3** are unexceptional and average 2.959(7) Å.

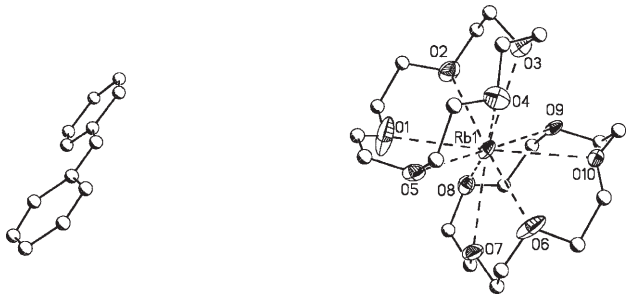

Figure 4. Crystal structure of **3**. Non-carbon atoms shown as thermal ellipsoids at 30% probability. Hydrogen atoms have been removed for clarity.

Following a similar line of investigation, replacement of [15]crown-5 by a crown ether of smaller diameter [12]crown-4 also affords a sandwich-type crown coordination under formation of separated ions, [Rb([12]crown-$4)_2$]-[$HCPh_2$] (**5**; see Figure 5). However, the small cavity size of [12]crown-4 prevents the effective encapsulation of the large metal cation, with the crown rings adopting a bent coordination with a metal–oxygen bond variation from 2.863(3) to 2.951(3) Å. Remarkably, one side of the cation remains exposed, but neither THF nor diphenylmethanide approach,

with the next nearest contact well beyond those to the carbon atoms in the crown ether (shortest Rb–C(crown) contact 3.58 Å to C24A), resulting in a gap of over 7 Å in the crystal lattice with no appreciable interactions on the naked face of the metal. Interestingly, despite this exposure of the metal center, the compound does not appear to be any more air or moisture sensitive than the other diphenylmethanides (all of which are exceedingly air and moisture sensitive and display pyrophoric character). Still, such double sandwich compounds combining large cations with crown ethers possessing small cavities are rare, with examples mainly limited to alkalides and electrides.[41,42] Other examples are limited to the recent silanides and germanides.[43]

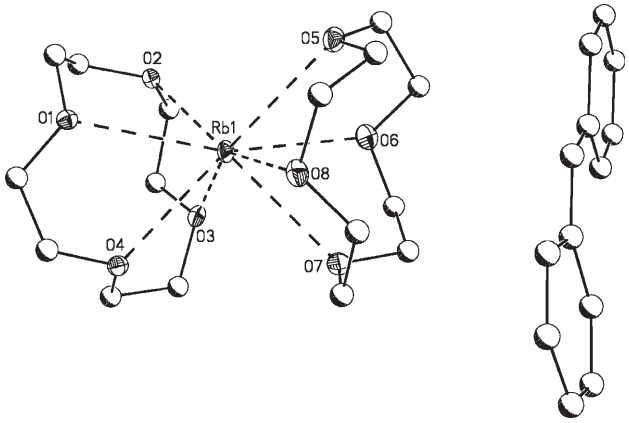

Figure 5. Crystal structure of **5**. Non-carbon atoms shown as thermal ellipsoids at 30% probability. Hydrogen atoms have been removed for clarity.

The structure dominating feature in both [K-[2.2.2]cryptand][$HCPh_2$] (**6**; Figure 6) and [Rb-[2.2.2]cryptand][$HCPh_2$] (**7**) is their charge-separated motif, with the cations snugly encapsulated by the cryptand. Almost no variation in metal–oxygen distances (2.801–2.832(7) Å for **6** and 2.8550–2.8821(9) Å for **7**) is observed. Likewise, the axial nitrogen connections are quite similar with 3.019(5) Å for **6** and 3.022(1) Å for **7**. Further increase of metal diameter does not allow for steric saturation using [2.2.2]cryptand. While the three-dimensional cryptand prevents coordination of a second macrocycle, coordination of a ligand leads to the formation of the contact structure **8** (Figure 7). In comparison to the separated ions **6** and **7**, the contact molecule displays slightly longer M–O/N bonds (O (equatorial) 2.897(4) Å; N (equatorial) 3.164(5) Å and 3.123(5) Å; O(axial) 3.771(5) Å). The cryptand is disordered such that in alternate conformations the apical bridge runs from the 1–4 to the 2–5 positions in the equatorial ring. The site occupancies are not equal; when positions 1 and 2 are occupied by nitrogen they undergo a slight conformational change of 0.26(1) Å to bring the ligand slightly closer to the metal center.

The three contact structures **8–10** share several common structural parameters, with **8** and **9** exhibiting η^3-metal–

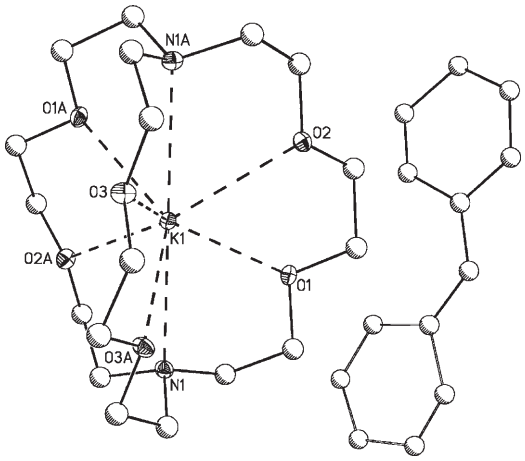

Figure 6. Crystal structure of **6**. Non-carbon atoms shown as thermal ellipsoids at 30% probability. Hydrogen atoms have been removed for clarity.

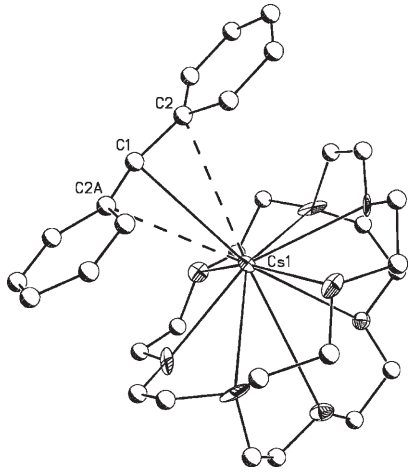

Figure 7. Crystal structure of **8**. Non-carbon atoms shown as thermal ellipsoids at 30% probability. Hydrogen atoms have been removed for clarity.

ligand coordination. Trends in bond lengths are primarily dictated by the increase in metal diameter, with a metal–ligand σ-bond of 3.302(8) for the cesium and 3.071(5) Å for the η^3-rubidium complex. Metal–ligand distances in the η^6-coordinated **10** are observed between 3.071(5) and 3.141(8) Å, respectively. The assignment of η^3 geometry for **8** and **9** stems from a comparison of metal–carbon bond length with Rb–C(2,8) in **9** observed at 3.311(3) and 3.393(3) Å. Beyond those, the closest Rb-C contact is 3.710(3) Å (C13). Severe disorder in **8** made this assignment more challenging, with Cs–C1 at 3.302(8) Å. The next shortest Cs–C distances are 3.517(8) (C2) and 3.584(8) Å (C2′) with C3′ at 3.685(8) and C7 at 3.849(8) Å. The assignment of η^6 coordination in **10** was made on the basis of a very narrow Rb–C bond lengths range (3.071(5) to 3.141(8) Å) to all six carbon atoms in the phenyl ring.

Anion geometry in **8–10** as represented by the C_{phenyl}-C_{ipso}-C_{phenyl} angles is very similar, averaging 132.6°. The

anions display close-to-planar geometry. Interestingly, the "flip" disorder is observed in the contact molecule **8**, with the anion exhibiting two opposing η^3 coordination motifs (Figure 1).

This disorder can be rationalized by the position of the metal in the center of the anion arrangement with π-interactions to each of the phenyl positions. One orientation of the anion is tipped slightly away from the metal center with a M–C1′ distance of 3.473(11) Å as compared to 3.302(8) Å in the opposing orientation. In all other respects, the anion geometry conforms to previously observed trends.

The contact molecule **8** is very similar to the metal–ligand binding mode observed in the low temperature modification (−23 °C) of the rubidium congener **9**, with [18]crown-6 completing the metal coordination sphere of the smaller metal. In contrast, crystals of the same reaction obtained at room temperature show a rubidium center with an η^6-metal–ligand coordination. The reproducible formation of η^3- and η^6-metal coordination at slightly different crystallization temperatures underscores the difficulties in predicting the metal coordination, a result further underscored by DFT calculations,[24] and further evaluated here.

Discussion

The solid-state structural motifs of compounds **1**–**10** include both separated ions and contact molecules. Most important in predicting their solid-state structures appears to be the understanding of factors governing steric saturation, either achieved by metal–crown, metal–solvent or metal–ligand interaction. This process is made more complex by the possibility of the metal and ligand binding via σ- and/or π-interactions, with π-bonding being possible with either only a part or the entire π-system. The simplest and best-understood principle in this analysis is the effect of crown ether (or cryptand) diameter on metal size. With a cavity size too small to fully encompass the cation, the need for further electrostatic stabilization can often not be filled by the organic ligand, resulting in the coordination of an additional crown ether to fill the metal coordination sphere. This arrangement typically results in separated ions. It is important to note that sandwich formation takes place regardless of initial reagent stoichiometry; this suggests the possibility that the coordinative stabilization provided by the crown ether versus energetic favorability of weakly bonding alkali organometallics is a major structure-determining criterion.

The contact molecules **8–10** involve the heavy alkali metals rubidium and cesium. Here, the large metal diameter makes steric saturation difficult to achieve. Moreover, metal–ligand bonding is weak. The small differences in bonding energy between the different metal–ligand/donor coordination modes, as well as energy differences between solvated and non-solvated forms have been analyzed using DFT methods and will be discussed below.

The delicate balance between the formation of contact molecules and separated ions is nicely illustrated in two rubidium compounds, where the use of [18]crown-6 leads to the contact structures **9** or **10** (depending on crystallization temperature), while utilization of the smaller [15]crown-5 requires a second crown ether to satisfy the coordinative environment (compound **3**) [Eqs. (4,5)]:

$$\mathrm{RbO}t\mathrm{Bu} + \mathrm{HCPh_2SiMe_3} \xrightarrow{[18]\text{crown-}6} [\mathrm{Rb}[18]\text{crown-}6][\mathrm{HCPh_2}] \quad (\mathbf{9}) \tag{4}$$

$$\mathrm{RbO}t\mathrm{Bu} + \mathrm{HCPh_2SiMe_3} \xrightarrow{2\,[15]\text{crown-}5} [\mathrm{Rb}\{[15]\text{crown-}5\}_2]^+[\mathrm{HCPh_2}]^- \quad (\mathbf{3}) \tag{5}$$

Because of their central role in our interest in studying metal–carbon binding, it is necessary to compare some representative structurally authenticated alkali metal diphenylides exhibiting direct metal−carbon bonds. (Table 2)

As expected, there is a smooth increase in $M–C_{ipso}$ distance in accordance with the increase in cation size, ranging from 2.63 Å for the $[Na(pmdta)(HCPh_2)]$ monomer[18] up to 3.30 Å for **8**, a clear trend despite changes in coordination number. In contrast, the tetrameric $[Na(tmeda)(HCPh_2)]_4$ displays extended bond lengths as compared to the PMDTA monomer. Likewise, the 12-coordinate η^6-[Rb[18]crown-6-(thf)][$CHPh_2$] (**10**) displays slightly longer M−C bond lengths (3.071(5)–3.141(8) Å) as compared to the nine-coordinate η^3-coordinated **9** (3.071(5) Å).

Several studies have examined the relationship between di- and triphenylmethanides of the alkali metals and the corresponding pyridylmethanes.[11–13] As a result, information on the nature of charge localization in the anion was gleaned. This trend is explained by noting that the polarizing power of the cation decreases with increasing size of the ion, and subsequently the ability of the metal to localize charge density at one point in the anion is reduced.[14] In the pyridyl analogues for both the diphenyl and trityl systems, the presence of the nitrogen in the ring draws a significant

Table 2. Bond lengths and angles in contact molecules of alkali metal diphenylmethanides.

Compound	M–C1 [Å]	C1–2, C1–8 [Å]	C8-C1-C2 [°]	M–O [Å]	M–N [Å]
$[Na(pmdta)][HCPh_2]$[a]	2.628(4)	1.423(6), 1.438(6)	132.02(4)		2.486(4), 2.422(4), 2.432(5)
	2.756(4)	1.446(7), 1.434(5)	132.06(5)		2.497(4), 2.426(4), 2.463(4)
$[Na(tmeda)(HCPh_2)]_4$[b]	2.72(1)	1.40(1), 1.45(1)	132.1(7)		
η^3-[Rb[18]crown-6][$HCPh_2$]	3.071(5)	1.422(5), 1.471(6)	132.6(3)	2.880(3)–2.989(3)	
η^6-[Rb[18]crown-6][$HCPh_2$]	3.141(8)	1.419(13), 1.423(13)	133.0(9)	2.766(17)–2.94(2), 2.921(9),2.960(3)	
[Cs[2.2.2]cryptand][$HCPh_2$][c]	3.302(8)	1.434(9)	132.2(9)	2.897(14)–3.005(3)	3.123(12), 3.164(19)

[a] Two independent anions. [b] Tetrameric structure; representative anion listed here. [c] Half anion is symmetry equivalent.

portion of charge density into that position, and coordination is exclusively through that point. Generally, it is well established that the potential energy surface for these compounds is very flat, with difficulties encountered in trying to assign minima.[14,29] This critically important observation implies that attempts to explain the structural features of the heavier alkali metal diphenylmethanides using simple electrostatic point charge models may not be adequate.

Increased coordination numbers coinciding with larger metal diameters often display an increased propensity for extended metal–ligand coordination through the phenyl rings of the ligand (via higher hapticity coordination η^3–η^6) starting from potassium and continuing through the heavier congeners. These softer cations prefer coordination to the diffuse anions preferentially over the smaller, more polarizing cations (Li^+, Na^+).[14,20,21] Indeed, in the trityl systems, low coordination numbers are favored for the smaller cations with the heavier congeners tending towards higher coordination and aggregation, with as many as 20 close contacts to the metal being observed.[14] In here we observe a greater propensity for the heavy cations to display contact molecules than has been predicted.[32]

In the heavy alkali metal contact diphenyl methanide structures discussed here, different trends as seen for the trityl TMEDA systems are observed. The presence of crown ethers and cryptands favors a higher coordination number within the aromatic system, while suppressing the propensity for aggregation. While one rubidium diphenylmethanide system **10** exhibits a modification experiencing higher hapticity as seen in the trityl system, no such metal–ligand binding is observed for the cesium analogue. Thus, several influences are in competition for the determination of the final structure: in addition to the known equilibrium between solvation and ligation that determines ion pairing in solution, one must consider the degree of delocalization of the anion (and thus the polarizing power of the cation) in addition to the electrostatic and steric contributions of the donor.

Solution behavior: ^{1}H and ^{13}C NMR solution studies suggest the formation of separated ions in solution since all compounds display little differentiation in chemical shift in both the ^{1}H and ^{13}C NMR spectra, a result obtained in both aromatic ([D_6]benzene) and polar solvents ([D_8]THF), a trend also verified in a recent series of alkali metal silanides and germanides.[43]

To investigate a possible temperature effect on the ion association, the contact molecules **9** and **10** were studied using variable temperature ^{1}H NMR spectroscopy. Using [D_8]toluene as a solvent, we investigated if the η^3- and η^6-binding modes observed in **9** and **10** are being maintained in solution. If the solid-state structure would be maintained, one would observe different NMR spectroscopic pattern. However, no such effects were observed, and upon cooling the solution, only peak-splitting as the result from inhibited phenyl rotation was visible.[24] These results support the existence of separated ions in solution and illustrate the general weakness of the metal-carbon bond.

Computational Studies

Computational studies were performed to examine the energetic contributions of the metal–donor and metal–anion interactions. These investigations expanded upon (and are superior to) those performed on the two previously communicated modifications [Rb[18]crown-6][$CHPh_2$] (**9**; η^3) and [Rb[18]crown-6(thf)][$CHPh_2$] (**10**; η^6).[24] Ignoring crystal packing interactions, the only chemical feature not shared between **9** and **10** is the THF molecule in the η^6 form, where crystal disorder yields fractional occupancies of two THF molecules with $O_{THF}\cdots$Rb separations of 3.143(4) Å (≈35% occup.) and 3.643(7) Å (≈65% occup.). In the absence of crystal packing, the increased solvation of Rb^+ by the THF oxygen atom could be argued as the origin of the η^6 form. In the crystal cell, the preferred binding arrangement of the contact structure, defined by the shape of the potential energy surface (PES) between Rb^+ and the π system of $[HCPh_2]^-$, must be weighed against the crystal interactions in the contact structure cavity. Theoretical considerations of the crystal packing interactions in these two modifications are made impractical due both to the computational resources required to adequately handle these large unit cells by periodic boundary conditions and by the simple fact that no large change in crystal packing would be expected given the constrained crystal geometry. This leaves the examination of the contact structures to isolated-molecule studies. The focus of these calculations is the interaction between Rb^+ and [$HCPh_2$], and the depth of the potential well across the surface of $[HCPh_2]^-$ as a function of Rb^+ solvation.

Methods: Density functional theory (DFT) calculations were performed on **9** and **10** and various related complexes using Gaussian 03[44] with the B3LYP hybrid density functional[45] and "ultrafine" grid size (program option, integration grid of 99 radial shells and 590 angular points per shell). The 6-31+G(d,p) Gaussian-type basis sets[46] were used for H, C, and O, while the Rb was treated with the LANL2DZ effective-core potential.[47] Geometry optimizations were performed both with (C_s symmetry in all cases) and without (from the η^3 and η^6 crystal geometries) symmetry restrictions at restricted Hartree-Fock/6-31G(d,p)/LANL2DZ (RHF) and, in some instances, B3LYP/6-31G(d,p)/LANL2DZ levels of theory to sample the PESs of the various complexes. Only those structures optimized at a RHF/6-31G(d,p)/LANL2DZ level of theory were characterized by normal mode analyses due to the size and structural range of these systems. In all non-symmetric optimizations, the final structures were energetically nearly identical (within 0.5 kJ mol^{-1}) to the C_s symmetry optimizations. Due to their resource-intensive nature and the shallow PESs of these contact structures, final DFT optimizations were performed only on the C_s symmetry forms of the complexes.

Results

Optimized structures: DFT geometry optimizations were performed on the C_{2v} symmetry $[HCPh_2]^-$ (Figure 8A) and the three C_s symmetry contact structures shown in Figure 8. Bond lengths relevant to the crystal structure analysis are provided in Table 3. Coordinate files for all optimized complexes are provided in the Supporting Information.

Unsolvated structures: The unsolvated Rb–$HCPh_2$ contact structure is marked by a curvature of the anion away from planarity (Figure 7B), bringing the phenyl rings closer to the Rb^+. The optimization of the C_s symmetry structure finds the Rb^+ interacting closely with the five centrally-located anion carbons and not directly above the methanide carbon; the complex is nominally η^5-coordinate. The binding energy for this structure is found to be 363.41 kJ mol^{-1}, with the change in shape of the $[HCPh_2]^-$ from its C_{2v} minimum corresponding to a 5.76 kJ mol^{-1} deformation energy.

Table 3. Structural data (distances in Angstroms, angles and dihedral angles in degrees), deformation energies, and binding energies (both in kJ mol^{-1}) for C_{2v} symmetry $[HCPh_2]^-$ (**A**), the two C_s symmetry Rb–$HCPh_2$ (geometry-unrestricted optimization (**B**) and optimization with the $[HCPh_2]^-$ forced to remain planar (**C**)), the two C_s symmetry ([18]crown-6)–Rb–$HCPh_2$ (**D** and **E**) and the two C_s symmetry (H_2O–[18]crown-6)–Rb–$HCPh_2$ contact structures (**F** and **G**). Structures and labeling schemes are shown in Figure 8.

	$[HCPh_2]^-$	Rb–$HCPh_2$	Rb–$HCPh_2$	([18]crown-6)–Rb–$HCPh_2$		(H_2O–[18]crown-6)–Rb–$HCPh_2$	
		Optimized	Planar	More stable	Less stable	More stable	Less stable
	A	B	C	D	E	F	G
C_1–C_2	1.4233	1.4282	1.4297	1.4282	1.4262	1.4282	1.4261
C_2-C_1-C_2'	133.69	132.30	132.81	133.16	133.37	133.06	133.35
C_3-C_2-C_1-C_2'	0.00	9.77	0.00	2.30	1.69	0.78	0.69
Rb–C_1		3.1671	3.1251	3.2962	3.3536	3.2547	3.3349
Rb–C_2		3.1846	3.2154	3.4290	3.4479	3.3630	3.4012
Rb–C_3		3.3374	3.3706	3.6381	3.5816	3.5690	3.5100
$r_{Rb-plane}$[a]			2.8524	3.1280	3.1023	2.9997	2.9845
Rb–O_1				3.1464	3.1900	3.1497	3.1589
Rb–O_2				3.0039	3.0551	3.0487	3.0828
Rb–O_3				3.1046	3.1177	3.1910	3.1929
Rb–O_4				3.0175	3.0168	3.1204	3.1152
Rb–O_{water}						3.7066	3.6598
O_3···O_{water}						3.1699	3.1758
ΔE $[HCPh_2]$[b]		5.76	0.74	1.23	1.21	1.75	1.63
$E_{binding}$[c]		363.41	358.03	265.99	265.33	252.80	252.57
$\Delta E_{more-less}$					6.64		0.22

[a] $r_{Rb-plane}$ = Average height of Rb above the plane of the $HCPh_2$ carbon atoms. See Figure 8. [b] The difference of the single-point energy of the $[HCPh_2]^-$ from each complex and the C_{2v} minimum energy anion. [c] Binding energy values were calculated from the minimum energy C_{2v} $[HCPh_2]^-$ and optimized Rb-solvated coordination fragments ([18]crown-6)–Rb^+ and (H_2O–[18]crown-6)–Rb^+.

A geometry optimization of Rb–$HCPh_2$ was also performed with the $[HCPh_2]^-$ forced to remain planar (Figure 7C), providing both a simplified system for the PES scans in the next section and a gauge of binding energy differences in the [18]crown-6 contact structures, where the anion is nearly planar. This plane-restricted structure is similar in many respects to B, with both the binding energy and anion deformation reduced by 5 kJ mol^{-1} and the η^5 coordination retained. As expected in this restricted optimization, the Rb^+ is brought closer to the single methanide carbon (C_1), the most negatively-charged carbon by natural bonding orbital (NBO) population analysis (total electron charges: C1: −0.406, C2: −0.046, C3: −0.298), and away from the C_2 and C_3 carbons.

Contact crown structures: The η^3 modification of Rb[18]crown-6–($CHPh_2$) can occur in two modifications displaying C_s symmetry, with the difference lying in the orientation of the crown ether with respect to the anion (Figure 7, D and E). This orientation difference corresponds to an absolute energy difference (D−E) of 6.64 kJ mol^{-1}, favoring the form observed in the crystal (D). The binding energies for these two forms are 265.9 (more stable conformation, D) and 265.3 (less stable, E) kJ mol^{-1}, nearly 100 kJ mol^{-1} lower than calculated for B. The $[HCPh_2]^-$ in these two complexes are deformed by only 1.23 (D) and 1.21 (E) kJ mol^{-1} relative to their C_{2v} minimum energy geometry (A).

H_2O-Coordinated structures: The H_2O replacement for the THF came from unexpected results in the RHF geometry optimizations. The optimization of the η^3[Rb[18]crown-6$HCPh_2$] (with the THF oxygen at the shorter O_{THF}–Rb distance) completed with the convergence of the η^6[Rb[18]crown-6(thf)$HCPh_2$] to a C_s-like (η^3) contact structure and complete dissociation of the THF. This same behavior was observed in DFT optimization attempts from the same starting structures. As THF does bind in $[Rb[18]crown-6]^+$ complexes in the absence of $[HCPh_2]^-$ (the coordinates of this B3LYP/6-31+G(d,p)/LANL2DZ cationic complex is provided in Supporting Information), the predicted dissociation is attributed to the steric repulsion between THF and [18]crown-6 being larger than the attractive interaction between the Rb^+ and THF oxygen atoms as the cation is coordinated at the center of the anion. This result, and how it provides for an explanation of the observed η^6 crystal form, is considered in the discussion.

The computationally expedient test for this steric influence is the calculation of a single H_2O molecule in replacement of the THF (with its oxygen at the O_{THF}–Rb = 3.143 Å starting position). The H_2O-bound complex was considered for both crown orientations in C_s symmetry and both H_2O orientations, where the water hydrogen atoms lie perpendicular to the mirror plane (F and G in Figure 7) and where the three H_2O atoms are in the reflection plane. The two forms where the H_2O atoms are in the reflection plane optimize with the formation of a single hydrogen bond to the nearest crown oxygen atom (O4) and O_{water}–Rb distances of 5.1949 (from the crown orientation in structure F) and 5.1657 (structure G) Å. These two forms do not represent binding motifs or distances as observed in the crystal and are not considered further. Optimizations of complexes F and G find the H_2O molecule of each forming two hydrogen bonds to nearest crown oxygen atoms (O_3···O_{water} in Figure 7). The two hydrogen bonds reduce the width of the crown cavity for the Rb^+ in both structures, pushing the

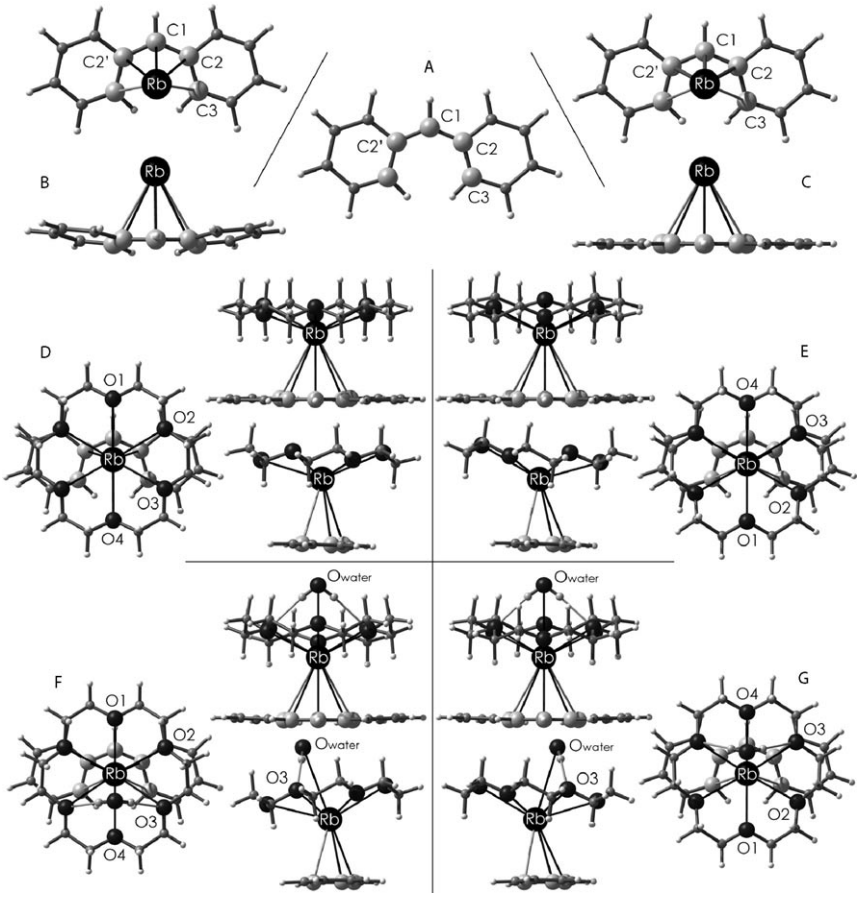

Figure 8. Optimized geometries and labeling schemes for C_{2v} symmetry $[HCPh_2]^-$ (**A**), the C_s symmetry Rb-$HCPh_2$ in optimized (**B**) and plane-restricted (**C**) forms, the two C_s symmetry η^3[Rb[18]crown-6$HCPh_2$] forms (**D** and **E**), and the two C_s symmetry ^{6}[Rb[18]crown-6(thf)$HCPh_2$] complexes, where the H_2O is aligned with the hydrogen atoms symmetry-related (**F** and **G**). The oxygen numbering schemes in (**D**, **E**, **F**, **G**) follow the trend in Rb–O distances and not the absolute arrangement with respect to the orientation of the $HCPh_2$. See Table 4. Images were generated with NanoEngineer-1[54] and POV-Ray.[55]

Rb^+ further below the crown plane. This structural change expectedly reduces the Rb-$HCPh_2$ distances slightly (Table 4). The effect of H_2O binding to the crown plane is a small reduction in total $[HCPh_2]^-$ binding energy (253 kJ mol^{-1}) and a slight increase in the $[HCPh_2]^-$ deformation energy (1.63 kJ mol^{-1}) relative to the two η^3[Rb[18]crown-6$HCPh_2$] conformations. The crown orientation observed in the η^3 crystal is again found to be the lower energy form (F), but the difference between conformations is only 0.22 kJ mol^{-1}. This small difference comes from geometry optimizations in a very shallow minimum. The fact that this energy is small is more important to the optimization comparisons than the actual energy itself.

The Rb–anion binding scan: DFT calculations predict that the η^3 form is favored for all contact structures and the η^6 modification with the bound THF is not predicted to be stable in vacuo. With the assumption that the calculations are accurately reproducing the experimental results (the binding energies and preferred positions may be density functional and/or basis set dependent, and the possibility exists that a very shallow η^6 local minimum is missed during the optimization process, but these dependences were not considered here), the focus of the binding preferences becomes the consideration of the packing influences on the observed crystal geometries. The goal of the isolated-molecule calculations in accounting for the crystal differences is then the determination of the change in contact structure energy that comes from the binding of the Rb^+ at non-equilibrium positions on the $[HCPh_2]^-$.

The PESs of C and D were sampled along a line perpendicular to the mirror plane of the C_s symmetry forms starting from the equilibrium position of Rb^+ in each structure (Figure 9). The resulting increases in energy from the equilibrium (η^3) positions are provided in Table 4.

The Rb^+ binding energies for C were calculated both from the plane-restricted Rb–plane optimum separation in C ($r_{Rb-plane}$ = 2.8524 Å) and the separation in D ($r_{Rb-plane}$ = 3.1280 Å) to consider the difference in interaction strength at two different heights and in the absence of the crown interactions. Over the 3.0 Å range, inclusion of the [18]-crown-6 leads to a 33 to 60% decrease in binding energy, with the difference reducing as the displacement from equilibrium increases. The two different crown orientations in C_s symmetry (D and E) are energeti-

Table 4. Binding energy differences of the Rb-$HCPh_2$ (**C**) and η^3[Rb[18]crown-6$HCPh_2$] (**D** and **E**, the results for both crown orientations are identical at the reported accuracy) as a function of cation position on the $[HCPh_2]^-$ surface. The selected positions are shown in Figure 8. $\Delta E_{Absolute}$ corresponds to the energy differences between the Rb–$HCPh_2$ contact structures at their 2.8524 Å (plane-restricted equilibrium) and 3.1280 Å ([18]crown-6 equilibrium Rb–plane separation) distances.

	Displacement	0.0	0.5	1.0	1.5	2.0	2.5	3.0
Rb−$HCPh_2$ ($r_{Rb-plane}$ = 2.8524, optimized)	$\Delta E_{binding}$	0.00	3.64	11.73	18.27	20.55	22.91	31.52
Rb−$HCPh_2$ ($r_{Rb-plane}$ = 3.1280, from [18]crown-6)	$\Delta E_{binding}$	0.00	1.54	5.23	9.07	12.14	16.09	23.56
Rb−$HCPh_2$ (2.8524)−Rb−$HCPh_2$ (3.1280)	$\Delta E_{Absolute}$	8.39	6.28	1.89	-0.82	-0.02	1.57	0.43
η^3[Rb[18]crown-6$HCPh_2$] (3.1280)	$\Delta E_{Binding}$	0.00	1.57	5.39	9.62	12.57	15.28	19.93

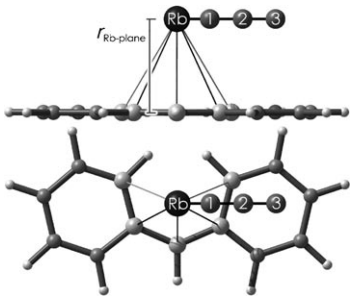

Figure 9. Rb-$HCPh_2$ and (18]crown-6)-Rb-$HCPh_2$ surface scan path and (integer) positions. See Table 4 for details. Images were generated with NanoEngineer-1[54] and POV-Ray.[55]

cally identical to two decimal places. At small displacements (0.0 to 2.0 Å), the changes in energy at the 3.1280 Å separation for both the unsolvated Rb^+ and $[Rb[18]crown\text{-}6]^+$ are very similar, as if the binding energy were only a function of Rb^+ separation. While this similarity might be considered as evidence that the crown and anion are not directly interacting, the absolute binding energies in these two cases differ by nearly 100 kJ mol^{-1} at their equilibrium positions and this energy difference does increase as the phenyl ring becomes more centrally located below the $[Rb[18]crown\text{-}6]^+$. The heights of Rb^+ above the $[HCPh_2]^-$ plane of the carbon atoms in these calculations bound the two average heights observed experimentally in the η^3 (3.0603 Å) and η^6 (3.0482 Å) modifications.

Computational discussion: The isolated-molecule calculations (both RHF and DFT attempts) predict that the THF-bound η^6 complex is not a stable minimum. The stronger binding of Rb^+ at the η^3 position not only directs the Rb^+ to the center of the anion, but the increase in Rb–$HCPh_2$ interaction strength alters the binding environment of the THF such that its coordination to Rb^+ is predicted to become weaker than the steric interactions between the THF and [18]crown-6. Assuming that the calculations are accurately describing the isolated complex and that no local η^6 contact structure would be stable in vacuo, it is left to the packing interactions in the crystal cell to explain the generation of this form. Given that the THF does not seem to bind to Rb^+ when the cation is sufficiently solvated/interacting strongly with the anion, the THF binding in the η^6 complex must be due to the Rb^+ interacting only with a phenyl ring and not, directly, with the full anion negative charge. With this diminished anion interaction, the $O_{THF}\cdots Rb$ interaction becomes stronger than the repulsive interactions between the THF and the crown. The THF–Rb^+ binding interaction is calculated to be 63.47 kJ mol^{-1} at a B3LYP/6-31+G(d,p)/LANL2DZ level of theory and is reduced to 29.89 kJ mol^{-1} in (THF–[18]crown-6)–Rb^+, making these interactions significant relative to *kT*, but far weaker than the cation-anion binding in any of the examined complexes. This anion position-dependent binding of the THF is supported, albeit with a very subtle structural change, by the position of the Rb^+ below the plane of its three closest-bound oxygen atoms in the crystal structures of η^3 (0.669(5) Å) and η^6 (0.445(6) Å). The positioning of the Rb^+ closer to the center of the crown plane in the η^6 form makes the cation more accessible for axial ligand binding opposite the anion position.

The H_2O-solvated structures do not directly aid in the analysis of Rb^+ solvation in the η^6 complex, but do demonstrate the extent to which the Rb^+ is a very weak (at best) lone pair acceptor when [18]crown-6-solvated Rb^+ is bound to $[HCPh_2]^-$ in an η^3 manner. In all four H_2O calculations, the $O_{THF}\cdots H_{water}$ hydrogen bonding interactions dominate over the $Rb\cdots O_{water}$ interactions in defining the final water positions. In the two H_2O-complex structures where all three atoms are in the C_s plane, the water orients such that the O_{water}-H···O(4) angle is nearly 180 degrees. In structures F and G, the O_{water}-Rb separation is partly a result of the two symmetry-restricted O_{water}-H···O(3) hydrogen bonds. These interactions, by their oval-shaped deformation (pinching) of the crown ring, position the Rb^+ for closer $[HCPh_2]^-$ binding, as noted by the reduced Rb–C_{anion} and increased Rb–O_{crown} distances. The improved Rb–$HCPh_2$ spatial interaction is offset by an effectively broken Rb–O_{water} and weakened Rb^+–[18]crown-6 interactions, leading to a net lowering of binding energy compared to complexes D and E.

The sensitivity of the binding energies in these complexes to the geometry is reflected, to an extent, in the difference between the trends reported in this work and the previous single-point energy calculations performed for η^3-[Rb[18]crown-6][$CHPh_2$] (**9**) and η^6-[Rb[18]crown-6(thf)]-[$CHPh_2$] (**10**).[24] Two different energy comparisons were performed using single-point energy calculations from crystal structure coordinates. The first was the binding energy difference of the η^3 form and the η^6 form without the THF molecule, enabling a comparison of the two Rb–$HCPh_2$ binding motifs. In this comparison, the η^3 form was favored at a RHF/6-31G(d,p) level of theory by 16.98 kJ mol^{-1}, while the η^6 form without its THF was favored at both B3LYP/6-31G(d,p) (16.35 kJ mol^{-1}) and BLYP/DNP (31.05 kJ mol^{-1}) levels of theory. The second comparison was of the THF-removed η^6 form and the separated THF molecule versus the complete η^6 complex, which was performed initially to determine the binding energy of the THF. Here, the two DFT calculations disagreed in the prediction of THF binding. The B3LYP/6-31G(d,p) energies indicated that the η^6 structure was more stable than the separate components by 9.85 kJ mol^{-1}, while the BYLP/DNP calculations predicted that the isolated η^6 and THF structures were more stable as separate species by 12.48 kJ mol^{-1}. The geometry optimizations performed in the current work are, by the fact that structures were allowed to locate minimum energy positions appropriate to the employed level of theory, more methodologically correct. The original single-point energy comparisons were performed from the crystal geometries due to the resource-intensive nature of even these calculations circa 2002. The current calculations do reinforce one aspect of the original findings, with the analysis here deemed a major improvement over the original work. The binding energies of

the anion in the crown-solvated Rb^+ complexes are reduced relative to the unsolvated cation, and this reduced binding energy comes with a broader range of motion across the anion surface. These results do not alone explain the observed η^3 and η^6 forms, but do provide a prediction of the minimum energy the crystal environment must contribute to the η^6 modification to counter the isolated-complex preference for η^3 binding. An estimate of this energy, which represents the minimum energy that the crystal lattice would need to contribute to stabilize the anion position in the absence of all other energy contributions, is approximately 20 kJ mol^{-1}.

Conclusion

Treatment of a silyl-substituted hydrocarbon with a heavy alkali metal *tert*-butoxide leads to the clean formation of alkali organometallics in high yield and purity, effectively circumventing the commonly observed difficulties of product separation in the widely used transmetallation reactions. The alkali (K, Rb, Cs) metal diphenylmethanides were treated with variously sized crown ethers as well as a cryptand to explore metal–ligand bonding trends. While solution studies indicate the exclusive formation of separated ions, contact molecules as well as separated ions were observed in the solid-state. Curiously, two different metal-ligand coordination modes (η^3 and η^6) were observed for a rubidium species, with consequent DFT studies to help understand the energy differences between the two.

DFT calculations of the η^3 and η^6 modifications predict that the THF-bound η^6 form is not a stable molecular complex, but that crown solvation does significantly reduce the binding energy of the Rb–$HCPh_2$ interaction. The reduction in direct Rb^+ solvation by the anion that comes with $[HCPh_2]^-$ displacement in the η^6 form is argued as the reason for the crystal binding of THF to Rb^+.

Experimental Section

All reactions were performed under vigorous exclusion of water and oxygen. $HCPh_2SiMe_3$ was prepared by the literature method.[25] Potassium *tert*-butoxide was purchased from Aldrich and used without further purification. Cesium and rubidium *tert*-butoxide were prepared by an adaptation of the literature method, refluxing the metal in toluene with addition of stoichiometric anhydrous *tert*-butanol, copious washing with hexane, and vacuum drying.[48] All other reagents and solvents were purified by standard procedures. Due to the pyrophoric nature of these compounds, satisfactory IR and elemental analysis could not be obtained. This is a well-established problem with alkali and alkaline earth organometallics.[5,49] All crystal data were collected using a Bruker SMART system, complete with 3-circle goniometer and APEX-CCD detector as described earlier.[50] The crystals were mounted on the diffractometer as described previously.[51] All crystal structures were solved using Patterson methods and were refined by full-matrix least-squares refinement on F^2.[52,53] All non-hydrogen atoms were refined anisotropically, except as noted otherwise. CCDC-214054–214061 contain the supplementary crystallographic data for this paper. These data can be obtained free of charge from The Cambridge Crystallographic Data Centre via www.ccdc.cam.ac.uk/data_request/cif.

General procedure for preparation of alkali diphenylmethanides: Solutions were prepared of MO*t*Bu (1.0 mmol) [M = K, Rb, Cs], $HCPh_2SiMe_3$ (1.0 mmol) and a crown ether (1.0 or 2.0 mmol) in hexane (10 mL). The acid solution was added dropwise to the MO*t*Bu slurry, followed by addition of the crown ether solution, which immediately gave a brilliant orange solution with a bright yellow precipitant. The mixture was stirred at 24 °C for 4 h, then THF added dropwise and the solution warmed gently to dissolve the solid product. The solution was stored at −23 °C, and yellow-orange crystals suitable for X-ray diffraction studies formed overnight.

[K[18]crown-6(thf)$_2$][HCPh$_2$] (1): Solutions were prepared of KO*t*Bu (0.14 g, 1.0 mmol), $HCPh_2SiMe_3$ (0.23 g, 1.0 mmol) and [18]crown-6 (0.23 g, 1.0 mmol) in hexane (10 mL). M.p. soften 95, melt 115–120 °C; yield: 0.48 g, (78.7 %); ^{1}H NMR (300 MHz, 25 °C, [D$_8$]THF): δ = 1.77 (t, THF), 3.55 (s, [18]crown-6, THF), 4.31 (s, *H*CPh$_2$), 5.59 (m, phenyl), 6.51 (m, phenyl), 7.17 (m, phenyl); ^{13}C NMR (300 MHz, 25 °C, [D$_8$]THF) δ = 25.49 (THF), 65.98 (THF), 68.90 ([18]crown-6), 79.19 (*C*HPh$_2$), 104.11, 115.58, 126.44, 144.66 (phenyl). Compound **1** crystallizes in the non-centrosymmetric space group $P2_1$. Data analysis using the PLATON protocol confirmed the non-centrosymmetric setting.[51] Crystal data for **1**: $KC_{33}H_{51}O_8$, M_r = 614.33, monoclinic, space group $P2(1)$, a = 12.8430(17), b = 18.425 (2), c = 15.264(2) Å; β = 112.384(2)°; V = 3339.8(6) Å^3, T = 97(2) K, Z = 4, μ = 0.206 mm^{-1}($Mo_{K\alpha}$); orange plates 0.80 × 0.40 × 0.2 mm^3; 18664 independent reflections (3.30 = 2θ = 62.00°); R_1 = 0.0631 for data $I > 2\sigma(I)$ and wR_2 = 0.1702 for all data.

[Cs$_2$([18]crown-6)$_3$][HCPh$_2$]$_2$ (2): Solutions were prepared of CsO*t*Bu (0.24 g, 1.0 mmol), $HCPh_2SiMe_3$ (0.23 g, 1.0 mmol) and [18]crown-6 (0.23 g, 1.0 mmol) in hexane (10 mL). M.p. 104–107 °C; yield: 0.15 g, (21.6 %); ^{1}H NMR (300 MHz, 25 °C, [D$_8$]THF): δ = 3.43 (m, [18]crown-6), 4.38 (s, *H*CPh$_2$), 5.68 (t, phenyl), 6.49, 6.61 (m, phenyl), 7.17 (m, phenyl); ^{13}C NMR (300 MHz, 25 °C, [D$_8$]THF): δ = 70.85 [18]crown-6, 81.76 (*C*HPh$_2$): δ = 106.60, 117.67, 129.27, 146.69 (phenyl). A section of the outer crown ether ring on Cs2 is slightly disordered and was modeled using two conformations. Crystal data for **2**: $Cs_2C_{62}H_{98}O_{18}$, M_r = 695.73, monoclinic, space group $P2(1)/c$, a = 27.240(3), b = 10.8426(14), c = 23.515(3) Å; β = 101.670(2)°; V = 6801.5(2) Å^3, T = 92(2) K, Z = 8, μ = 1.136 mm^{-1} ($Mo_{K\alpha}$); orange blocks 0.40 × 0.30 × 0.30 mm^3; 24181 independent reflections (3.30 = 2θ = 66.00°); R_1 = 0.0498 for data $I > 2\sigma(I)$ and wR_2 = 0.0785 for all data.

[Rb([15]crown-5)$_2$][HCPh$_2$] (3): Solutions were prepared of RbO*t*Bu (0.16 g, 1.0 mmol), $HCPh_2SiMe_3$ (0.26 g, 1.0 mmol) and [15]crown-5 (0.48 g, 2.0 mmol) in hexane (15 mL). M.p. 133–135 °C; yield: (0.3 g, 43.3 %); ^{1}H NMR (300 MHz, 25 °C, [D$_8$]THF): δ = 3.66(s, [18]crown-6), 5.51 (m, *H*CPh$_2$), 6.52 (m, phenyl), 7.18–7.28 (m, phenyl); ^{13}C NMR (300 MHz, 25 °C, [D$_8$]THF) δ = 69.22 [18]crown-6, 40.34 (*C*HPh$_2$), 124.45, 126.84, 127.41, 140.04 (phenyl). Crystal data for **3**: $RbC_{33}H_{51}O_{10}$, M_r = 693.21, monoclinic, space group $P2(1)/c$, a = 8.9603(10), b = 15.5206(18), c = 24.663(3) Å; β = 96.841(2)°; V = 3405.5(7) Å^3, T = 96(2) K, Z = 4, μ = 1.508 mm^{-1} ($Mo_{K\alpha}$) yellow blocks 0.6 × 0.4 × 0.35 mm^3; 7817 independent reflections (3.30 = 2θ = 55.00°); R_1 = 0.0574 for data $I > 2\sigma(I)$ and wR_2 = 0.0881 for all data.

[K([15]crown-5)$_2$][HCPh$_2$] (4): Solutions were prepared of KO*t*Bu (0.23 g, 2.0 mmol), $HCPh_2SiMe_3$ (0.49 g, 2.0 mmol) and [15]crown-5 (0.6 g, 2.9 mmol) in THF (15 mL). M.p. soften 95, melt 139.5–140.5 °C; yield: (0.17 g, 12.3 %); ^{1}H NMR (300 MHz, 25 °C, [D$_8$]THF): δ = 3.57 (s, [18]crown-6), 3.95 (s, *H*CPh$_2$), 6.55 (t, phenyl), 7.13–7.25 (m, phenyl); ^{13}C NMR (300 MHz, 25 °C, [D$_8$]THF) δ = 40.35 (*C*HPh$_2$), 69.20 [18]crown-6, 124.45, 126.70, 127.41, 140.04 (phenyl).

[Rb([12]crown-4)$_2$][HCPh$_2$] (5): Solutions were prepared of RbO*t*Bu (0.16 g, 1.0 mmol), $HCPh_2SiMe_3$ (0.25 g, 1.0 mmol) and [12]crown-4 (0.32 g, 2.0 mmol) in hexane (10 mL). M.p. 175–177 °C; yield: 0.39 g, (64.0 %); ^{1}H NMR (300 MHz, 25 °C, [D$_8$]THF): δ = 3.49 ([12]crown-4), 4.39 (s, *H*CPh$_2$), 5.68 (m, phenyl), 6.54 (m, phenyl), 6.48–6.59 (m, phenyl); ^{13}C NMR (300 MHz, 25 °C, [D$_8$]THF): δ = 66.19 (crown), 79.44 (*C*HPh$_2$), 104.70, 116.46, 126.45, 144.61 (phenyl). Crystal data for **5**: $RbC_{29}H_{43}O_8$, M_r = 605.10, triclinic, space group $P\bar{1}$, a = 10.881(1), b =

10.949(1) $c=13.779(2)$ Å; $V=3163.7(5)$ Å^3, $\alpha=105.048(2)$, $\beta=97.845(2)$, $\gamma=107.281(2)°$; $T=96(2)$ K, $Z=2$, $\mu=1.728$ mm^{-1} ($Mo_{K\alpha}$); orange needles $0.80\times0.50\times0.05$ mm^3; 8453 independent reflections ($3.30=2\theta=60.00°$); $R_1=0.0523$ for data $I>2\sigma(I)$ and $wR_2=0.1323$ for all data.

[K[2.2.2]cryptand][HCPh$_2$] (6): Solutions were prepared of KO*t*Bu (0.14 g, 1.0 mmol), $HCPh_2SiMe_3$ (0.25 g, 1.0 mmol) and [2.2.2]cryptand (0.38 g, 1.0 mmol) in hexane (10 mL). M.p. 113–114.5 °C; yield: 0.42 g, (72.0 %); ^{1}H NMR (300 MHz, 25 °C, [D$_8$]THF): $\delta=2.47$ (t, NCH_2CH_2O), 3.49 (t,NCH_2CH_2O), 3.51 (s, OC_2H_4O), 4.25 (s, *H*CPh$_2$), 5.48 (m, phenyl), 6.41 (m, phenyl), 7.15 (m, phenyl); ^{13}C NMR (300 MHz, 25 °C, [D$_8$]THF): δ = 55.11 (NCH_2CH_2O), 68.45 (NCH_2CH_2O), 70.93 (OC_2H_4O), 81.80 (*C*HPh$_2$), 105.38, 126.31, 128.70, 142.52 (phenyl). Crystal data for **6**: $KN_2C_{32}H_{44}O_6$, $M_r=582.81$, monoclinic, space group $C2/c$, $a=26.727(4)$, $b=8.2065(17)$, $c=19.367(3)$ Å; $\beta=133.311(2)°$; $V=3091.0(8)$ Å^3, $T=96(2)$ K, $Z=4$, $\mu=0.216$ mm^{-1}($Mo_{K\alpha}$; orange needles $0.35\times0.20\times0.10$ mm^3; 4521 independent reflections ($3.30=2\theta=60.00°$); $R_1=0.0386$ for data $I>2\sigma(I)$ and w$R_2=0.0975$ for all data.

[Rb[2.2.2]cryptand][HCPh$_2$] (7): Solutions were prepared of RbO*t*Bu (0.17 g, 1.0 mmol), $HCPh_2SiMe_3$ (0.25 g, 1.0 mmol) and [2.2.2] cryptand (0.38 g, 1.0 mmol) in hexane (10 mL). M.p. 108.0–111.0 °C; yield: 0.38 g, (60.3 %); ^{1}H NMR (300 MHz, 25 °C, [D$_8$]THF): $\delta=2.36$ (t, NCH_2CH_2O), 3.36 (t,NCH_2CH_2O), 3.41 (s, OC_2H_4O), 4.25 (s, *H*CPh$_2$), 5.45 (m, phenyl), 6.38 (m, phenyl), 7.10 (m, phenyl); ^{13}C NMR (300 MHz, 25 °C, [D$_8$]THF): δ = 53.20 (NCH_2CH_2O), 66.56 (NCH_2CH_2O), 69.21 (OC_2H_4O), 79.83 (*C*HPh$_2$), 105.55, 116.30, 125.83, 145.01 (phenyl). Crystal data for **7**: $RbN_2C_{31}H_{48}O_6$, $M_r=630.18$, monoclinic, space group $C2/c$, $a=26.760(3)$, $b=8.2510(10)$, $c=19.318(6)$ Å; $\beta=133.282(2)°$; $V=3105.1(6)$ Å^3, $T=90(2)$ K, $Z=4$, $\mu=1.639$ mm^{-1} ($Mo_{K\alpha}$; orange needles $0.40\times0.35\times0.05$ mm^3; 4528 independent reflections ($3.30=2\theta=60.00°$); $R_1=0.0275$ for data $I>2\sigma(I)$ and $wR_2=0.0631$ for all data.

Cs[2.2.2]cryptand(HCPh$_2$) (8): Solutions were prepared of CsO*t*Bu (0.21 g, 1.0 mmol), $HCPh_2SiMe_3$ (0.25 g, 1.0 mmol) and [2.2.2]cryptand (0.38 g, 1.0 mmol) in hexane (10 mL). M.p. 131.0–133.5 °C; yield: 0.07 g, (10.2 %); ^{1}H NMR (300 MHz, 25 °C, [D$_8$]THF): $\delta=1.74$ (t, NCH_2CH_2O), 2.74 (t,NCH_2CH_2O), 2.81 (s, OC_2H_4O), 3.71 (s, *H*CPh$_2$), 4.95 (m, phenyl), 5.87 (m, phenyl), 6.48 (m, phenyl); ^{13}C NMR (300 MHz, 25 °C, [D$_8$]THF): δ = 56.77 (NCH_2CH_2O), 69.70 (NCH_2CH_2O), (70.93 (OC_2H_4O), 81.70 (*C*HPh$_2$), 106.48, 117.46, 128.72, 146.72 (phenyl). Crystal data for **8**: $CsN_2C_{32}H_{44}O_6$, $M_r=685.60$, orthorhombic, space group $Cmc2(1)$, $a=19.843(2)$, $b=9.2486(8)$, $c=17.239(2)$ Å; $V=3163.7(5)$ Å^3, $T=96(2)$ K, $Z=4$, $\mu=1.215$ mm^{-1} ($Mo_{K\alpha}$; orange needles $0.70\times0.20\times0.05$ mm^3; 4685 independent reflections ($3.30=2\theta=60.00°$); $R_1=0.0308$ for data $I>2\sigma(I)$ and $wR_2=0.0724$ for all data.

Acknowledgements

This work was supported by the National Science Foundation (CHE-0108098 and CHE0505863). Purchase of the X-Ray diffractometer was made possible with grants from NSF (CHE-95-27898) and the W. M. Keck Foundation and Syracuse University. D.G.A. thanks the Intelligence Community Postdoctoral Research Fellowship Program (ICPRFP) for computational research support.

[1] J. D. Smith, *Adv. Organomet. Chem.* **1999**, *43*, 267.
[2] E. Weiss, *Angew. Chem.* **1993**, *105*, 1565; *Angew. Chem. Int. Ed. Engl.* **1993**, *32*, 1501.
[3] P. von Ragué Schleyer, C. Schade, *Adv. Organomet. Chem.* **1991**, *27*, 169.
[4] P. von Ragué Schleyer, *Pure Appl. Chem.* **1984**, *56*, 151.
[5] P. Andrews, K. Henderson, K. Ruhlandt-Senge, in *Comprehensive Organometallic chemistry III, Vol. II* (Eds.: R. H. Crabtree, D. M. P. Mingos), Elsevier, Oxford, **2006**, pp. 1–66.
[6] See for example: a) S. Harder, S. Müller, E. Hübner, *Organometallics* **2004**, *23*, 178
[7] M. Schlosser, *Pure Appl. Chem.* **1988**, *60*, 1627.
[8] P. von Ragué Schleyer, *Pure Appl. Chem.* **1983**, *55*, 355.
[9] W. J. Hehre, L. Radom, P. von Ragué Schleyer, J. Pople, *Ab initio Molecular Orbital Theory*, Wiley, New York, **1986**.
[10] A. J. Streitwieser, *Acc. Chem. Res.* **1984**, *17*, 353.
[11] D. Stalke, U. Pieper, *Organometallics* **1993**, *12*, 1201.
[12] D. Stalke, H. Gornitzka, *Organometallics* **1994**, *13*, 4398.
[13] D. Stalke, M. Pfeiffer, G. Bertrand, C. Hemmert, H. Gornitzka, *Organometallics* **2000**, *19*, 112.
[14] D. Hoffman, W. Bauer, P. von Ragué Schleyer, U. Pieper, D. Stalke, *Organometallics* **1993**, *12*, 1193.
[15] P. von Ragué Schleyer, W. Bauer, F. Hampel, N. J. R. v. Eikema Hommes, P. Otto, U. Pieper, D. Stalke, D. S. Wright, R. Snaith, *J. Am. Chem. Soc.* **1994**, *116*, 528.
[16] M. A. Beno, H. Hope, M. Olmstead, P. P. Power, *Organometallics* **1985**, *4*, 2117.
[17] C. Schade, P. von Ragué Schleyer, H. Dietrich, W. Mahdi, *J. Am. Chem. Soc.* **1986**, *108*, 2484; Schleyer, H. Dietrich, W. Mahdi, *J. Am. Chem. Soc.* **1986**, *108*, 2484.
[18] S. Corbelin, J. Kopf, N. P. Lorenzen, E. Weiss, *J. Organomet. Chem.* **1991**, *415*, 293.
[19] P. P. Power, M. Olmstead, *J. Am. Chem. Soc.* **1985**, *107*, 2174.
[20] J. J. Brooks, G. D. Stucky, *J. Am. Chem. Soc.* **1972**, *94*, 7333.
[21] H. Koster, E. Weiss, *J. Organomet. Chem.* **1979**, *168*, 273.
[22] H. Viebrock, U. Behrens, T. Panther, E. Weiss, *J. Organomet. Chem.* **1995**, *491*, 19.
[23] D. M. Jenkins, W. Teng, U. Englich, K. Ruhlandt-Senge, D. Stone, *Organometallics* **2001**, *20*, 4600.
[24] J. S. Alexander, K. Ruhlandt-Senge, B. Hudson, D. G. Allis, *J. Am. Chem. Soc.* **2003**, *125*, 15002.
[25] M. S. Hill, P. B. Hitchcock, *Organometallics* **2002**, *21*, 220.
[26] F. Uhlig, R. Hummeltenberg, *J. Organomet. Chem.* **1993**, *452*, C9.
[27] F. Uhlig, K. Ruhlandt-Senge, K. Hassler, U. Englich, *Inorg. Chem.* **1998**, *37*, 3532.
[28] C. Marschner, *Eur. J. Inorg. Chem.* **1998**, *2*, 221.
[29] R. J. Bushby, H. L. Steel, M. P. Tytko, *J. Chem. Soc. Perkin Trans. 2* **1990**, *7*, 1155.
[30] J. S. Alexander, K. Ruhlandt-Senge, *Chem. Eur. J.* **2004**, *10*, 1274.
[31] R. D. Shannon, *Acta Crystallogr. Sect. A* **1976**, *32*, 751.
[32] C. Lambert, P. v. R. Schleyer, *Angew. Chem.* **1994**, *106*, 1187; *Angew. Chem. Int. Ed. Engl.* **1994**, *33*, 1129.
[33] J. L. Vidal, R. C. Schoening, J. M. Troup, *Inorg. Chem.* **1981**, *20*, 227.
[34] G. Pilet, S. Cordier, C. Perrin, A. Perrin, *Inorg. Chim. Acta* **2003**, *350*, 537.
[35] T. Akutagawa, K. Shitagami, S. Nishihara, S. Takeda, T. Hasegawa, T. Nakamura, Y. Hosokoshi, K. Inoue, S. Ikeuchi, Y. Miyazaki, K. Saito, *J. Am. Chem. Soc.* **2005**, *127*, 4397.
[36] K. V. Domasevitch, J. A. Rusanova, O. Yu. Vassilyeva, V. N. Kokozay, P. J. Squattrito, J. Sieler, P. R. Raithby, *J. Chem. Soc. Dalton Trans.* **1999**, 3087.
[37] K. V. Domasevitch, V. V. Ponomareva, E. B. Rusanov, *J. Chem. Soc. Dalton Trans.* **1997**, 1177.
[38] K. V. Domasevitch, J. A. Rusanova, O. Y. Vassilyeva, V. N. Kokozay, P. J. Squattrito, J. Sieler, P. R. Raithby, *J. Chem. Soc. Dalton Trans.* **1999**, 3087.
[39] G. Pilet, S. Cordler, C. Perrin, A. Perrin, *Inorg. Chim. Acta* **2003**, *350*, 537.
[40] J. J. Vidal, R. C. Schoening, J. M. Troup, *Inorg. Chem.* **1981**, *20*, 227.
[41] R. H. Huang, J. L. Eglin, S. Z. Huang, L. E. H. McMills, J. L. Dye, *J. Am. Chem. Soc.* **1993**, *115*, 9542.
[42] R. H. Huang, S. Z. Huang, J. L. Dye, *J. Coord. Chem.* **1998**, *46*, 13.
[43] a) W. Teng, K. Ruhlandt-Senge, K. *Organometallics* **2004**, *23*, 952; b) W. Teng, K. Ruhlandt-Senge, *Organometallics* **2004**, *23*, 2694; c) W. Teng, K. Ruhlandt-Senge, *Chem. Eur. J.* **2005**, *11*, 2462.
[44] Gaussian 03, Revision D.01, G. W. T. M. J. Frisch, H. B. Schlegel, G. E. Scuseria, M. A. Robb, J. R. Cheeseman, J. A. Montgomery, Jr., T. Vreven, K. N. Kudin, J. C. Burant, J. M. Millam, S. S. Iyengar, J. Tomasi, V. Barone, B. Mennucci, M. Cossi, G. Scalmani, N. Rega, G. A. Petersson, H. Nakatsuji, M. Hada, M. Ehara, K. Toyota, R. Fukuda, J. Hasegawa, M. Ishida, T. Nakajima, Y. Honda, O. Kitao,

H. Nakai, M. Klene, X. Li, J. E. Knox, H. P. Hratchian, J. B. Cross, V. Bakken, C. Adamo, J. Jaramillo, R. Gomperts, R. E. Stratmann, O. Yazyev, A. J. Austin, R. Cammi, C. Pomelli, J. W. Ochterski, P. Y. Ayala, K. Morokuma, G. A. Voth, P. Salvador, J. J. Dannenberg, V. G. Zakrzewski, S. Dapprich, A. D. Daniels, M. C. Strain, O. Farkas, D. K. Malick, A. D. Rabuck, K. Raghavachari, J. B. Foresman, J. V. Ortiz, Q. Cui, A. G. Baboul, S. Clifford, J. Cioslowski, B. B. Stefanov, G. Liu, A. Liashenko, P. Piskorz, I. Komaromi, R. L. Martin, D. J. Fox, T. Keith, M. A. Al-Laham, C. Y. Peng, A. Nanayakkara, M. Challacombe, P. M. W. Gill, B. Johnson, W. Chen, M. W. Wong, C. Gonzalez, J. A. Pople, Gaussian, Inc, Wallingford CT, **2004**.

[45] A. D. Becke, *J. Chem. Phys.* **1993**, *98*, 5648.

[46] R. D. W. J. Hehre, J. A. Pople, *J. Chem. Phys.* **1972**, *56*, 2257.

[47] W. R. W. P. J. Hay, *J. Chem. Phys.* **1985**, *82*, 270.

[48] E. Weiss, H. Alsdorf, *Z. Anorg. Allg. Chem.* **1970**, *372*, 206.

[49] T. P. Hanusa, *Comprehensive Organometallic chemistry III, Vol. II* (Eds.: R. H. Crabtree, D. M. P. Mingos), Elsevier, Oxford, **2006**, pp. 67–152.

[50] S. Chadwick, K. Ruhlandt-Senge, *Chem. Eur. J.* **1998**, *4*, 1768.

[51] H. Hope, *Prog. Inorg. Chem.* **1994**, *41*, 1.

[52] G. M. Sheldrick, ShelxTL, **1994**, Bruker Analytical X-ray Instruments, Madison, WI, **1994**.

[53] A. L. Spek, 1.07 ed., Utrecht, **1990**.

[54] NanoEngineer-1, v.a8. Nanorex, Inc., **2006**.

[55] Persistence of Vision Raytracer (POV-Ray), v3.6. Persistence of Vision Raytracer Pty. Ltd., **2006**.

Received: May 21, 2007
Published online: September 21, 2007

